Evolution of Filament Structures during Edge-Localized Modes in the MAST Tokamak

A. Kirk,[1] B. Koch,[2,3] R. Scannell,[1,4] H. R. Wilson,[5] G. Counsell,[1] J. Dowling,[1] A. Herrmann,[3] R. Martin,[1] M. Walsh,[1] and the MAST team

[1]*EURATOM/UKAEA Fusion Association, Culham Science Centre, Abingdon, Oxon OX14 3DB, United Kingdom*
[2]*Institut für Physik der Humboldt—Universität zu Berlin, Germany*
[3]*Max-Planck-Institut für Plasmaphysik, EURATOM Association, Garching, Germany*
[4]*Department of Electrical and Electronic Engineering, University College Cork, Association EURATOM-DCU, Ireland*
[5]*University of York, Heslington, York YO10 5DD, United Kingdom*

(Received 14 February 2006; published 10 May 2006)

Edge-localized modes (ELMs) are repetitive instabilities that occur in the outer region of tokamak plasmas. This Letter provides new information on and the implications of the evolution of the filament structures observed during ELMs in the MAST tokamak. The filaments exist for the time over which particles are being released into the scrape off layer. They start off at the plasma edge rotating at the velocity of the pedestal, and then decelerate toroidally and accelerate radially outwards. As the filaments propagate radially they remain aligned with the local magnetic field line.

DOI: 10.1103/PhysRevLett.96.185001 PACS numbers: 52.35.Py, 52.55.Fa

The high confinement mode [1], or H mode, is the standard operating regime envisaged for future tokamaks such as ITER [2]. It is achieved because a narrow (~5% of the minor radius), insulating region, or transport barrier, forms at the plasma edge. This edge transport barrier gives rise to steep edge pressure gradients, which can drive instabilities known as edge-localized modes (ELMs) [3]. So called type-I ELMs result in the sudden release of 5%–15% of the stored energy in a short amount of time (100–300 μs), which results in large heat fluxes to plasma facing components [4]. Understanding the size, poloidal and toroidal localization, and the outward radial extent of ELMs is crucial in order to calculate their effect on power loading both on the first wall and the divertor target plates in future devices [2].

Filament structures have been observed during ELMs in a wide range of tokamaks using a variety of diagnostics (see [5] and reference therein). Although it is clear that these structures exist during the ELM, it is still unclear how long they last for and how they propagate. The reason for the uncertainty is that it has not been possible to follow the three-dimensional propagation of the filaments as a function of time. It is important to remove this uncertainty in order to discriminate between models that try to predict the amount of energy lost due to an ELM. These models range from those where the filaments are the main loss mechanism to those where the filaments exist only for a short time and serve only to slow the edge rotation and result in a collapse back to L mode. In this Letter, for the first time the 3D propagation of filaments through an ELM will be presented using visible imaging on the MAST [6] tokamak (at Culham Science Centre, U.K.) and the consequence for ELM energy loss models will be discussed.

The unique wide angle view of the plasma and the large gap (> 50 cm) between the last closed flux surface (LCFS) and the vessel in MAST allows the radial propagation of the filaments to be tracked without interactions with vessel components. The aim of this study is to determine the evolution of the filaments by capturing several images of the entire plasma during a single ELM. In order to do this we have used a Hadland Imacon 468 camera which is capable of recording up to 6 consecutive images. The image separation used was between 5 and 20 μs and the exposure time was in the range 5 to 10 μs. The choice of exposure time is a trade off between the available light and the blurring of the filaments due to their movement.

Since only one set of 6 frames can be recorded per plasma discharge, a trigger based on the currents arriving at the divertor targets has been used to ensure that the images are captured during an ELM. Figure 1(a) shows the time trace of the target D_α light and the current to the divertor (determined by measuring the voltage across a shunt resistor connecting the divertor target to the vessel) as a function of time from the start of the ELM (defined here as the time at which the midplane D_α signal increases by 10% of the value at the ELM peak). It is the negative peak in the current at the start of the ELM, presumably due to the arrival of fast electrons at the target, which is used as the basis of the trigger and allows images to be obtained within 40 μs of the start of the ELM. The camera is preprogrammed to obtain images at varying times from this trigger. The results presented in this Letter are based on sets of 6 images from 8 type-I ELMs.

Figures 1(b)–1(d) show the visible light images (mainly D_α) obtained using a 10 μs exposure at 67, 77, and 87 μs, respectively, from the start of the ELM. Clear filamentary structures are observed. The observed filaments are spread uniformly over toroidal angle showing that they are not features associated with, for example, in vessel components.

The images have been analyzed by mapping 3D field lines onto the 2D image, taking account of the lens distortion, using a technique similar to that described in

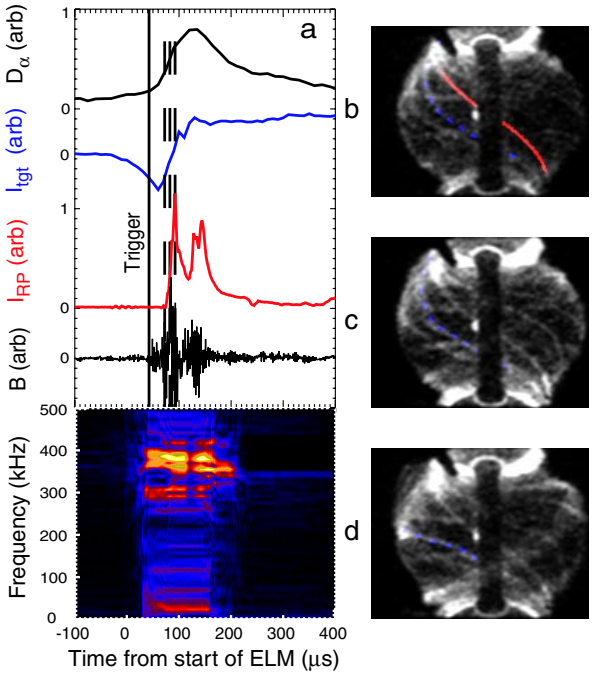

FIG. 1 (color online). (a) The target D_α, current to the divertor target, midplane ion saturation current, magnetic fluctuation signal, and spectrogram as a function of time relative to the start time of the ELM (defined in the text). (b)–(d) are visible light images of the MAST plasma separated by 10 μs with a 10 μs exposure at the location of the dashed vertical lines in (a).

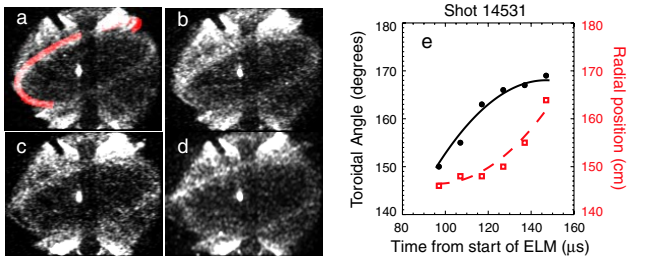

FIG. 2 (color online). (a)–(d) Visible light images of the MAST plasma obtained at times of 117, 127, 137, and 147 μs after the start of an ELM. (e) The toroidal and radial location of one of the filaments as a function of time during the ELM.

Ref. [7]. Using the magnetic equilibrium, the 3D field lines are generated at various toroidal angles and distances outside the LCFS (ΔR_{LCFS}) in steps of 2 cm. These field lines are then projected onto the image, and the difference between the mapped field line and the observed filament is minimized. In order to test the accuracy of this method, simulated images have been generated with filaments at known radii and angle. The field lines have then been fitted using the above techniques. It has been found that the toroidal position can be determined to within $\pm 2°$ and the radius to an accuracy of ± 2 cm. The width of the solid red line shown in Fig. 1(b) [Fig. 2(a)] represents $\pm 2°$ ($\pm$ 2 cm), which gives a visual indication of how accurately a field line can be aligned toroidally (radially) with a filament. To test if the filaments are aligned with the field line, we have generated lines modifying the toroidal field in 10% steps from the nominal value to $\pm 30\%$. This gives qualitatively different field lines compared to just changing the radius. The filaments are found to be aligned with the local field line (i.e., agree with the local pitch angle within $\sim 10\%$) for all values of ΔR_{LCFS} and for nearly all poloidal angles between the X points. However, because of diagnostic limitations it is not possible to say what happens close to the X point, in particular, whether the filaments are attached to the core.

The propagation of the filaments can be determined by measuring their toroidal and radial location in subsequent frames. For example, 7 filaments have been observed in Fig. 1(b) located at toroidal angles of 48° (dashed blue line), 95°, 119°, 190°, 235°, 282°, and 350° (solid red line) and all have $\Delta R_{\mathrm{LCFS}} < 4$ cm. The toroidal angle is defined at the midplane ($z = 0$) such that 0° is at the back and 90° at the left-hand edge. The toroidal separation of the filaments implies a toroidal mode number of <15, and taking into account the rotation of the filaments during the exposure time, each filament has a width perpendicular to the field line of ~ 5 cm. As the filaments expand out radially their toroidal width, after correction for the rotation, remains constant within the measurement errors. In Fig. 1(c) 6 filaments are clear enough to be analyzed at toroidal locations of 57° (dashed blue line), 103°, 195°, 243°, 289°, and 355°. This is consistent with the filaments rotating toroidally between 5° and 9° in the cocurrent direction; i.e., filaments at the far side of the plasma move from right to left from one image to the next. This corresponds to a toroidal velocity of 12 to 22 km s^{-1}. The filaments have also expanded radially such that ΔR_{LCFS} is between 2 and 6 cm.

Finally, in Fig. 1(d) filaments are visible at 60° (dashed blue line), 200°, 289°, and 359°, i.e., the toroidal rotation is now smaller, between 0° and 5°. Although most of the filaments have $\Delta R_{\mathrm{LCFS}} < 6$ cm, the filament at 60° (dashed blue line) has expanded radially such that $\Delta R_{\mathrm{LCFS}} = 13$ cm. In fact, this filament has expanded so far that it has interacted with the midplane reciprocating probe, which can be observed as the bright spot on the left-hand side of the image. The radial position of this filament determined from the field lines agrees well with the known position of the probe $\Delta R_{\mathrm{LCFS}} = 12$ cm. The interaction of the filament with the probe can be observed in the ion saturation current trace shown in Fig. 1(a). There is a second peak observed in this trace 38 μs later. If this peak was due to another filament, and a rotation of between 5° and 9° every 10 μs is assumed, then this other filament should be observable at an angle of 26°–41°. This is consistent with the toroidal mode number of ~ 15, but no filament can be clearly seen in the image. Further information on the nature of the filaments can be obtained by studying the magnetic fluctuations measured by a coil located 5 cm further back inside the head of the reciprocating probe head. As can be seen from Fig. 1(a), a clear

magnetic signal is observed correlated with the peaks in the ion saturation current, i.e., with the arrival of the filament at the probe. The spectrogram of this signal [Fig. 1(a)] shows that the dominant frequency component is centered at ~380 kHz. This frequency is much higher than the diamagnetic drift frequency for the densities and temperatures of the filament (typically 10–50 kHz) but is similar to the Alfvén frequency (300–600 kHz). This suggests that the fluctuations have an electromagnetic origin.

The radial expansion of the filaments can be most clearly observed when the filaments are located at the near side of the plasma. Figures 2(a)–2(d) show such an example. Four filaments are analyzable in Fig. 2(a) at toroidal locations of 37°, 104°, 163°, and 205° and the implied toroidal mode number is ~8. The field line describing the filament at 163° and $\Delta R_{\mathrm{LCFS}} < 2$ cm is superimposed on Fig. 2(a). In the next frame [Fig. 2(b)], which is 10 μs later, this filament has moved toroidally by 3° and radially by ~2 cm. Another 10 μs later the toroidal angle has hardly changed but the filament has moved radially so that it is no longer attached to the plasma near to the midplane. The radial expansion continues to increase as can be seen in Fig. 2(d). The toroidal and radial position of this filament over the 6 frames recorded is shown in Fig. 2(e). The toroidal velocity decreases from ~13 to 2 km s^{-1} while the radial velocity increases from 2 km s^{-1} to 9 km s^{-1}. Superimposed on Fig. 2(e) are curves representing a toroidal deceleration of 2.2×10^8 ms^{-2} from 10 km s^{-1} at 90 μs and a radial acceleration from zero of $\sim 1.2 \times 10^8$ ms^{-2}.

The latest image obtained for any of the 8 ELMs studied was 200 μs after the start of the ELM, and in this image filaments could still be seen. In a single ELM, not all the filaments have identical behavior; i.e., radial velocity and distance from the LCFS can be different. However, all the filaments appear to remain attached near to the LCFS for at least 50 μs, sometime after this the filaments individually detach. The number of *visible* filaments decreases with time (typically from 7 to 2), which could be either because the actual number decreases or because they become less visible as the number of particles in them decreases. The implied toroidal mode number varies from 8 to 17. For each ELM studied, the calculated toroidal velocity of every filament is found to decrease with time. The filaments start rotating in the same direction and with approximately the same toroidal velocity as the plasma just inside the top of the pedestal. This suggests that the filaments remain magnetically connected to this region at least until the toroidal rotation starts to decrease. The mean deceleration of the filaments is $(1.7 \pm 0.4) \times 10^8$ ms^{-2} which is consistent with the change in toroidal impurity velocities at the pedestal of $\sim 1 \times 10^8$ ms^{-2} previously measured using visible Doppler spectroscopy [8].

The visible images give information on the space-time structure of the ELM. However, it is difficult to unfold from them any information on the density or temperature of the filaments. Information on this and further evidence for the time evolution of the ELM filament comes from data from the new multitime point edge Nd-YAG Thomson scattering system on MAST. The laser is aligned radially at the midplane. The spatial resolution in the edge region is ~1 cm and each Nd-YAG laser can fire once every 20 ms. The timing of the four lasers has been set such that four electron density and temperature radial profiles can be produced with a 5 μs delay between them during a single ELM.

Figures 3(a) and 3(b) show the edge density and temperature profiles of a case where a filament is in the line of sight of the diagnostic. The timing of the laser pulses relative to the target D_α light is shown in Fig. 3(c); they are separated by 5 μs starting 53 μs after the start of the ELM. The first density profile (red open circles) shows the formation of an outboard tail. The electron temperature in this tail is ~70 eV, which is hotter than the scrape off layer (SOL) (~20 eV) but not as hot as the pedestal (~150 eV). The second profile (green solid squares) obtained 5 μs later shows that the density perturbation has expanded radially by ~2 cm corresponding to a radial expansion velocity of 4 km s^{-1}. Density profiles obtained during other ELMs where the line of sight is not through a filament show effectively no change to the edge gradient or position of the LCFS during the 15 μs over which the profiles are obtained; hence this shows that the perturbations to the edge of the plasma are localized to the location of the filaments. The fact that there is an increase in density in the SOL with apparently no local decrease in density at the

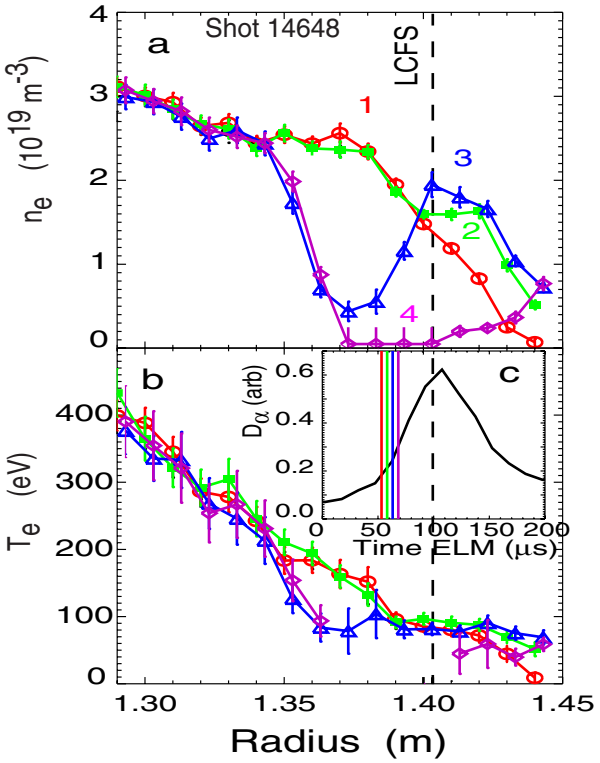

FIG. 3 (color online). The time evolution of (a) the edge density profile and (b) the edge temperature profile for a single ELM. (c) The target D_α signal as a function of time.

pedestal suggests that at this stage there is a nonlocalized source of particles into the filament; i.e., it is not a blob of plasma detaching but is an extended flux tube which connects back into the plasma, possibly near to the X point.

The third density profile (open blue triangles) shows a sudden change in the profile; the filament has detached from the LCFS leaving a depression behind in the density profile. The electron temperature in this detached filament remains around 80 eV. Assuming that the filament has a circular cross section and extends between upper and lower X points, the number of particles in each filament represents only 2.5% of the number of particles and 1.5% of the energy expelled by the ELM. Hence even with 10 filaments the total particle and energy loss observed can not be accounted for by models which state that the ELM is just the breaking off of filaments of plasma from the core. The depression in the density profile must be localized, first because if it were extended toroidally and poloidally it would account for a change in the measured plasma density of $\sim$15%, inconsistent with the total observed change in density from the entire ELM duration of $\sim$4%. Second, as was stated above holes were not observed in profiles where the line of sight of the system does not intersect a filament. A possible explanation is that the filament extends both inside and outside the LCFS and a reconnection event leads to this filament of plasma being expelled leaving behind it a localized depression in the density profile that would subsequently be filled in by parallel transport. Similar ''holes'' have been observed in 2D Thomson scattering profiles obtained during an ELM on ASDEX Upgrade [9].

In the final profile the filament has expanded radially by at least 5 cm corresponding to a radial expansion velocity of 10 km s^{-1}. This is consistent with the expansion velocities observed from the visible images after the filament has detached. By the time the filaments reach the midplane probe ($\Delta R_{\mathrm{LCFS}} = 12$ cm) the typical electron temperatures are $\sim$40–60 eV and the densities are ~ 4–6×10^{18} m^{-3}. This indicates that by this stage the source of particles and energy into the filaments has either been removed or has drastically reduced.

The new results presented in this Letter show clearly for the first time that the filaments observed during ELMs persist for $\sim$200 μs. These filaments start off rotating toroidally at $\sim$30 km s^{-1}, which is similar to the rotation speed of the pedestal region. The toroidal rotation slows, and as it does so, the filaments accelerate radially outwards. As the filaments propagate radially they follow the direction of the local field line and remain approximately constant in width. This together with the fact that there is a magnetic signature associated with the filaments may suggest that they carry a current. The filaments appear to be attached to the core for at least 50 μs; sometime after this the filaments detach from the midplane. The detached filaments do not contain enough particles or energy to account for the changes associated with the ELM. Filaments appear to behave individually in their radial propagation; i.e., the filaments detach at different times.

Based on these observations the most probable ELM energy loss process is as follows: for the first 50–100 μs filaments remain near to the LCFS, rotate toroidally with the plasma, and are aligned with the field lines. This is consistent with the predictions of the nonlinear theory of the ballooning instability [10]. During this period 50%–75% of the total ELM particle (ΔN_{ELM}) and energy (ΔW_{ELM}) loss occurs presumably due to an increase in transport across the perturbed field lines associated with the filaments. After this time the filaments accelerate radially away from the LCFS. Since their measured density and temperature decrease with distance, it suggests that a reconnection event has occurred and that the filaments no longer remain attached to the core. At the time of the reconnection each filament contains up to 2.5% of ΔN_{ELM} and ΔW_{ELM}, which is subsequently lost by parallel transport along open field lines to the targets.

The fact that filaments are observed for $\sim$200 μs (which is comparable to the ELM energy loss time found by SOL transport simulations used to model the temporal evolution of the power arriving at the targets) suggests that the ELM energy loss is associated with filaments. Although models exist for calculating the evolution of the energy in detached filaments [11], there has not previously been a measure of the content of the filament at detachment. The measurements obtained in this Letter can be used as an input to such models to allow the power loading to the wall as a function of distance from the plasma to be calculated.

UKAEA authors were funded jointly by the United Kingdom Engineering and Physical Sciences Research Council and by the European Communities under the contract of Association between EURATOM and UKAEA.

[1] F. Wagner *et al.*, Phys. Rev. Lett. **49**, 1408 (1982).
[2] ITER Physics Expert Group, Nucl. Fusion **39**, 2391 (1999).
[3] J. W. Connor, Plasma Phys. Controlled Fusion **40**, 531 (1998).
[4] A. Loarte *et al.*, Plasma Phys. Controlled Fusion **44**, 1815 (2002).
[5] A. Kirk *et al.*, Plasma Phys. Controlled Fusion **47**, 995 (2005).
[6] B. Lloyd *et al.*, Nucl. Fusion **43**, 1665 (2003).
[7] G. S. K. Fung *et al.*, Opt. Eng. (Bellingham, Wash.) **42**, 2967 (2003).
[8] A. Kirk *et al.*, Plasma Phys. Controlled Fusion **47**, 315 (2005).
[9] B. Kurzan *et al.*, Phys. Rev. Lett. **95**, 145001 (2005).
[10] H. R. Wilson and S. C. Cowley, Phys. Rev. Lett. **92**, 175006 (2004).
[11] W. Fundamenski *et al.*, Plasma Phys. Controlled Fusion **48**, 109 (2006).